Theory of optically excited intrinsic semiconductor quantum dots

Y. Z. Hu, M. Lindberg, and S. W. Koch
Department of Physics and Optical Sciences Center, University of Arizona, Tucson, Arizona 85721
(Received 20 November 1989)

The influence of the Coulomb interaction on one and two electron-hole-pair excitations in semiconductor quantum dots is analyzed. Using a numerical matrix-diagonalization scheme, the energy eigenvalues and the eigenfunctions of the relevant states are computed. Significant deviations from the strong-confinement approximation are observed. It is shown that the biexciton binding energy increases with decreasing dot size. This result is verified using third-order perturbation theory for small quantum dots. The optical properties of the quantum dots are computed, and it is shown that the Coulomb interaction significantly influences the allowed dipole transitions, causing increasing two-pair absorption on the high-energy side of the decreasing one-pair absorption. Surface-polarization effects are studied for quantum dots embedded in another dielectric medium.

I. INTRODUCTION

Semiconductor microcrystallites are often denoted as "quantum dots" (QD's) when the crystallite size is of the order of or less than the exciton Bohr radius. The three-dimensional quantum-confinement effects in these quantum dots lead to pronounced modifications of the electronic and optical properties.[1-17] Already, the first studies[1-3] showed that the small radius of quantum dots makes the allowed states for excited electron-hole pairs discrete. In the linear-optical-absorption spectra of ideal quantum dots the single electron-hole-pair (EHP) states should appear as spectrally isolated peaks. Resonance structures have indeed been observed in experiments, but the different peaks are relatively broad and spectrally overlapping.[2-5,10,13] These effects are a direct consequence of the relatively large homogeneous broadening and the size distribution of the crystallites in currently available samples.

In order to theoretically analyze the linear- and nonlinear-optical properties of quantum dots, one has to compute the properties of the one- and two-EHP states. Since the problem of two electron-hole pairs in a confining geometry cannot be solved analytically, the published calculations are based on variational approaches[11] or other approximation schemes[9] which lead to partially contradictory conclusions. In order to obtain reliable results, in this paper we develop a numerical procedure which allows to accurately study the one- and two-pair states in our model for small quantum dots. The details of this quantum-dot model are outlined in Sec. II. Our numerical matrix diagonalization is described in Sec. III. As a result of these calculations we obtain the energies and eigenfunctions of all the relevant one- and two-EHP states. In Appendix A we supplement these numerical calculations by third-order perturbation calculations which are valid for small dot radii. As a result of these investigations we find that the Coulomb interaction causes significant modifications of the one- and two-pair eigenfunctions. In Sec. IV we use these eigenfunctions to compute the linear- and nonlinear-optical properties of the quantum dots. As one of the most striking features we find that two-pair states in quantum dots lead to an increasing probe absorption on the high-energy side of the one-EHP resonances.

II. MODEL OF A QUANTUM DOT AND ITS EXCITATIONS

We investigate semiconductor quantum dots having sizes which are of the same order of magnitude as the Bohr radius of the exciton in the corresponding bulk material, typically between 10 and 150 A. As direct consequence of this *mesoscopic* size, the boundaries in quantum dots have an important effect on the physical properties. In our model we assume that a real sample containing quantum dots can be considered as an ensemble of mutually independent dots. In order to obtain the optical properties, it is therefore sufficient to study only single quantum dots for different radii. For simplicity, we idealize the shape of a QD as simple sphere.[1,2] The great symmetry chosen simplifies the calculations and is not expected to introduce significant qualitative deviations of the results.

To model the electronic excitations in a QD we assume that the effective-mass approximation can be adapted.[1,2] This means that the QD is macroscopic in comparison to the unit cell of the material but not in comparison to the Bohr radius of the exciton. The boundary of the QD, however, restricts the possible energy states available for the electrons and holes. The motion of the electrons and holes inside the dot is described with the many-body electron-hole Hamiltonian which we use in the position representation. Electrons and holes interact via the Coulomb interaction, which is modified in comparison to bulk semiconductors because of the presence of induced dielectric surface charges.[2] The basic Hamiltonian is given by

$$\hat{H}=\hat{H}_e+\hat{H}_h+\hat{V}_{e\text{-}e}+\hat{V}_{h\text{-}h}+\hat{V}_{e\text{-}h}+\hat{W}\ ,$$

where

$$\hat{H}_e=\sum_s \int dr\, \psi_e^\dagger(r,s)\left[E_g-\frac{\hbar^2}{2m_e}\nabla^2\right]\psi_e(r,s)\ ,$$

$$\hat{H}_h=\sum_s \int dr\, \psi_h^\dagger(r,s)\left[-\frac{\hbar^2}{2m_h}\right]\nabla^2\psi_h(r,s)\ ,$$

$$\hat{V}_{e\text{-}e}=\frac{1}{2}\sum_{ss'} \int\int dr\, dr' \psi_e^\dagger(r,s)\psi_e^\dagger(r',s')V(r-r')\psi_e(r',s')\psi_e(r,s)\ , \tag{1}$$

$$\hat{V}_{h\text{-}h}=\frac{1}{2}\sum_{ss'} \int\int dr\, dr' \psi_h^\dagger(r,s)\psi_h^\dagger(r',s')V(r-r')\psi_h(r',s')\psi_h(r,s)\ ,$$

$$\hat{V}_{e\text{-}h}=-\sum_{ss'} \int\int dr\, dr' \psi_e^\dagger(r,s)\psi_h^\dagger(r',s')V(r-r')\psi_h(r',s')\psi_e(r,s)\ ,$$

and $\psi_e(r,s),\psi_h(r,s)$ is the annihilation operator of an electron, hole with spin s at position r, respectively. $\hat{W}$ is the correction to the Coulomb interaction due to the surface polarization of the quantum dots. The explicit form of $\hat{W}$ is given in the appendix of Ref. 9 and will not be repeated here.

The boundary conditions at the surface of the QD require that the field operators vanish outside the dot, i.e.,

$$\psi_e(r,s)=\psi_h(r,s)=0 \quad \text{when } |r|\geq R\ ,$$

where R is the radius of the sphere. The spin index has the values $-\frac{1}{2}$ and $\frac{1}{2}$. The field operators obey the usual anticommutation rules. Notice, that the total numbers of both electrons and holes with given spin are constants of motion under the Hamiltonian (1), because the operators

$$\hat{N}_e=\int dr\, \psi_e^\dagger(r,s)\psi_e(r,s)\ ,$$
$$\hat{N}_h=\int dr\, \psi_h^\dagger(r,s)\psi_h(r,s) \tag{2}$$

commute with $\hat{H}$.

Once we know the state structure of our system by solving the eigenvalue problem given by the Hamiltonian (1), we can couple the system to a light field. We describe this coupling with the interaction Hamiltonian

$$\hat{H}_{\text{int}}=-E(t)P^+ +\text{H.c.}$$
$$=-p_{cv}E(t)\sum_s \int dr\, \psi_e^\dagger(r,s)\psi_h^\dagger(r,s)+\text{H.c.}\ , \tag{3}$$

where we used the rotating-wave approximation and included only interband transitions, the interband matrix element being denoted by p_{cv}. To obtain the optical properties of the QD we must calculate the expectation value of the polarization operator $\langle P^+\rangle$ from which we can extract the optical susceptibility. For this purpose we need the matrix elements of P^+ between the eigenstates. Notice that the operator P^+ creates electron-hole pairs and, hence only those states, which have equal number of electrons and holes are optically coupled. For our problem, all other eigenstates of the Hamiltonian (1) are irrelevant.

Because of the spherical symmetry of the QD and because of the fact that the interaction between the particles only depends on the relative positions, one can show that the total angular momentum operator relative to the center of the dot,

$$\hat{L}=\hat{L}_e+\hat{L}_h=\sum_s \int dr\, \psi_e^\dagger(r,s)\hat{L}(r)\psi_e(r,s)$$
$$-\sum_s \int dr\, \psi_h^\dagger(r,s)\hat{L}(r)\psi_h(r,s)\ , \tag{4}$$

where $\hat{L}(r)=\mathbf{r}\times\nabla$, is a constant of motion under the Hamiltonian (1). The operator $\hat{L}$ also commutes with the interaction Hamiltonian (3) and therefore only states with total angular momentum quantum number $L=0$ are optically active, as long as only optical interband transitions are allowed. When we also include intraband transitions, $\hat{L}$ no longer commutes with the Hamiltonian. The property that only states with $L=0$ couple optically is familiar from the bulk case where only s excitons are dipole allowed. Similarly, we see that the operator for the z component of the total spin is a constant of motion under the Hamiltonians (1) and (3). Therefore, only states with total spin equal to zero are optically coupled.

The eigenfunctions of the Hamiltonian (1) can be classified according to the number of electrons and holes in each state. Even though the interaction Hamiltonian (3) only describes the creation of electron-hole pairs, it turns out that the single-particle states provide a useful basis to analyze the properties of the QD. In the following, we outline the relevant properties of the single-electron states. The eigenvalue problem is given by

$$\hat{H}|\Psi_e\rangle=E|\Psi_e\rangle\ , \tag{5}$$

where the eigenfunction $|\Psi_e\rangle$ has the general form

$$|\Psi_e\rangle=\sum_s \int dr\, \phi(r,s)\psi_e^\dagger(r,s)|0\rangle\ . \tag{6}$$

Here $|0\rangle$ is the vacuum state without particles. Using the Hamiltonian and the anticommutation rules we obtain the differential equation

$$-\frac{\hbar^2}{2m_e}\nabla^2\phi(r,s)=(E-E_g)\phi(r,s) \tag{7}$$

for the single-particle wave functions $\phi(r,s)$. The solution of this equation with the boundary condition

$$\phi(r,s)=0 \quad \text{for } |r| \geq R$$

is

$$\phi_N(r,s)=\left[\frac{2}{R^3}\right]^{1/2}\frac{j_l(\alpha_{nl}|r|/R)}{j_{l+1}(\alpha_{nl})}Y_{lm}(\theta,\Phi)\delta_{\sigma s} \tag{8}$$

with

$$\begin{aligned} &N=\{n,l,m\} \\ &n=1,2,3,\ldots, \\ &l=0,1,2,\ldots, \\ &m=-l,-l+1,\ldots,l-1,l\ , \\ &\sigma=-\tfrac{1}{2},\tfrac{1}{2}\ , \\ &E_N=\frac{\hbar^2}{2m_e}\left[\frac{\alpha_{nl}}{R}\right]^2=\left[\frac{a_{eB}}{R}\right]^2 E_{eR}\alpha_{nl}^2\ , \end{aligned} \tag{9}$$

j_l is the lth-order spherical Bessel function, α_{nl} is its nth root, and Y_{lm} is a spherical harmonic function. The variables $|r|$, θ, and Φ are the spherical coordinates of the vector r. E_{eR} and a_{eB} are Rydberg energy and Bohr radius evaluated using the mass of the electron. The single-particle wave functions and energies for the holes are obtained by replacing the electron mass everywhere by the hole mass and neglecting E_g. Consequently, the single-particle wave functions for electrons and holes are equal. The single-particle energies (9) in quantum dots form discrete levels,[1,2] in contrast to the well-known case of bulk semiconductors, where one has a continuum. Notice that the spacing between the levels increases like R^{-2} with decreasing radius.

We know from the case of bulk semiconductors that Coulomb effects are very important for the pair states, e.g., leading to the existence of the exciton. At this point, the important aspect in which quantum dots differ from bulk material is that we have the additional length scale R in the dots. A crude estimate shows that the single-particle energies increase like R^{-2} and the Coulomb interaction energy grows like R^{-1} when the radius R decreases. So the relative importance of the Coulomb energy decreases in comparison to the confinement energy. In the so-called strong-confinement approximation,[1,7] the Coulomb interaction is completely neglected and the electrons and holes are taken as free particles in the dot. This is a good first approximation to estimate the pair energies in QD's with a radius clearly smaller than the Bohr radius of the exciton. However, this approximation may lead to wrong conclusions in some points, especially, where energy differences or details of the electron-hole wave functions are involved. The strong-confinement approximation yields wrong selection rules for the optical transitions and, of course, all binding energies are exactly zero. To avoid these shortcomings in this paper we therefore treat the Coulomb interaction exactly for the relevant states.

As long as the energy spacing between the single-particle states is larger than the Coulomb interaction energy, the states are not very strongly mixed and we do not have the volume problem encountered when computing dipole matrix elements in bulk systems. It is therefore meaningful to consider only the few lowest eigenstates, i.e., one-pair and two-pair states, to obtain the third-order optical response for the system. We refer to these one-pair and two-pair states loosely as exciton and biexciton states, respectively.

Since the spatial part and the spin part of the wave functions are not correlated we can always write the total functions as products of these parts and normalize them independently. The exciton (one-pair) state has the general form

$$|\Psi_1\rangle=\int\int dr_e dr_h \phi^{(1)}(r_e,r_h) \times\sum_{s_e s_h}\chi(s_e,s_h)\psi_e^\dagger(r_e,s_e)\psi_h^\dagger(r_h,s_h)|0\rangle\ . \tag{10}$$

In the same way as for the single-particle states, we obtain the differential equation

$$\left[-\frac{\hbar^2}{2m_e}\nabla_e^2-\frac{\hbar^2}{2m_h}\nabla_h^2-V(r_e-r_h)\right]\phi^{(1)}(r_e,r_h) =(E_1-E_g)\phi^{(1)}(r_e,r_h) \tag{11}$$

for the one-pair wave function $\phi^{(1)}$. Here, the boundary condition is that $\phi^{(1)}$ vanishes when $|r_e|$ or $|r_h|$ is larger or equal to R. The spin functions χ in Eq. (10) can be freely chosen. The normalization of the state (10) yields the condition

$$\langle\Psi_1|\Psi_1\rangle=\int\int dr_e dr_h|\phi^{(1)}(r_e,r_h)|^2\sum_{s_e s_h}|\chi(s_e,s_h)|^2=1\ .$$

In the case of bulk semiconductors, Eq. (11) can be simplified considerably since the equations for relative and center-of-mass motion of the electron-hole pair separate. In a QD, however, this separation is not possible and Eq. (11) must be solved directly. For the general case, exact analytical solutions are not known and we have to use numerical methods. However, in the strong confinement approximation where the Coulomb term is neglected, the solution of Eq. (11) is obtained in terms of products of single-particle functions. Simultaneously, the energies are then simply the corresponding sums of the single-particle energies. The binding energy of the ground-state exciton, defined as

$$\delta E_1=\left[\frac{a_B}{R}\right]^2 E_R\pi^2-E_1\ , \tag{12}$$

vanishes in the strong confinement approximation. In Eq. (12), a_B and E_R are the exciton Bohr radius and Rydberg energy in the corresponding bulk semiconductor, respectively.

The generalization of Eq. (11) to biexciton states is relatively straightforward. We can use the fact that the spatial coordinates and the spin are uncorrelated to write the eigenfunctions in the general form

$$|\Psi_2\rangle=\int\int\int\int dr_{e_1}dr_{e_2}dr_{h_1}dr_{h_2}\phi^{(2)}(r_{e_1},r_{e_2},r_{h_1},r_{h_2}) \times\sum_{s_{e_1}s_{e_2}s_{h_1}s_{h_2}}\chi(s_{e_1}s_{e_2}s_{h_1}s_{h_2})\psi_e^\dagger(r_{e_1},s_{e_1})\psi_e^\dagger(r_{e_2},s_{e_2})\psi_h^\dagger(r_{h_1},s_{h_1})\psi_h^\dagger(r_{h_2},s_{h_2})|0\rangle \ .$$

For the two-pair wave function $\phi^{(2)}$ we then obtain the equation

$$\left[-\frac{\hbar^2}{2m_e}(\nabla_{e_1}^2+\nabla_{e_2}^2)-\frac{\hbar^2}{2m_h}(\nabla_{h_1}^2+\nabla_{h_2}^2)-V(r_{e_1}-r_{h_1})-V(r_{e_2}-r_{h_2})-V(r_{e_1}-r_{h_2})-V(r_{e_2}-r_{h_1}) +V(r_{e_1}-r_{e_2})+V(r_{h_1}-r_{h_2})\right]\phi^{(2)}(r_{e_1},r_{e_2},r_{h_1},r_{h_2})=(E_2-2E_g)\phi^{(2)}(r_{e_1},r_{e_2},r_{h_1},r_{h_2}) \ . \quad (13)$$

Equations (11) and (13) are written without the surface polarization term $\hat{W}$, which, however, can be included trivially when needed. The normalization of the biexciton state is

$$1=\langle\Psi_2|\Psi_2\rangle=4\sum_{s_{e_1}s_{e_2}s_{h_1}s_{h_2}}\int\int dr_{e_1}dr_{e_2}dr_{h_1}dr_{h_2}|\phi^{(2)}(r_{e_1},r_{e_2},r_{h_1},r_{h_2})|^2|\chi(s_{e_1}s_{e_2}s_{h_1}s_{h_2})|^2$$

when the total coefficient $\phi\chi$ is assumed to be antisymmetric in the exchange of electrons or holes. This can always be assumed because only the antisymmetric part gives contribution in $|\Psi_2\rangle$. The binding energy of the ground-state biexciton is defined relative to the ground-state energy of two excitons as

$$\delta E_2=2E_1-E_2 \ . \quad (14)$$

Again, δE_2 is exactly zero in the strong-confinement approximation.

III. NUMERICAL MATRIX DIAGONALIZATION

In this section we discuss our numerical scheme to compute the eigenvalues and eigenfunctions of the one- and two-pair states. We use direct matrix diagonalization for dot radii of the order of, or smaller than, the bulk exciton Bohr radius. For comparison, and to have an independent check, we also study the region around zero radius using ordinary perturbation theory,[14] which converges well in this limit. The perturbative treatment is outlined in the Appendix.

To solve the differential equations (11) and (13) we expand the respective eigenfunctions into a complete set of basis functions. For the one-pair problem, Eq. (11), we choose the basis functions as a set of product functions in the form

$$\Phi_{N,N'}^{(1)}(r_e,r_h)=\phi_N(r_e)\phi_{N'}(r_h) \ , \quad (15)$$

where ϕ_N are the single-particle wave functions, Eq. (8), and N is again the short-hand notation for the set of quantum numbers $\{n,l,m\}$. Correspondingly, the expansion for the two-pair functions $\Phi^{(2)}$ is chosen in terms of products of four functions (two for electrons and two for holes). The functions ϕ are the single-particle wave functions obtained in the previous section. Note, that the spin index has been suppressed because the energies are independent of the spin. The total eigenfunctions must then have the spin part included. For the regime $R\cong a_B$ or smaller, the kinetic-energy contributions, which give the diagonal elements, dominate over the Coulomb contributions which give the off-diagonal elements. Therefore, since we only want to compute the eigenfunctions and energies of the few lowest states, it is a rapidly converging procedure to take a finite matrix to represent the total, infinite matrix. The obtained results are then checked by increasing the size of the finite matrix.

The calculations are greatly simplified by the fact that the total angular momentum is a constant of motion and therefore provides a good quantum number, L. The one- and two-pair eigenstates must be also eigenstates of the total angular momentum. To reduce the complexity of numerical calculations, we do not use the sets $\{\Phi^{(1)}\}$ and $\{\Phi^{(2)}\}$ directly. Instead, a unitary transformation is applied to obtain a new basis, in which the total angular momentum is already diagonal. As shown in the previous section, for optical interband transitions we have to consider only the states with $L=0$, since the vacuum state has $L=0$. For the energy states we can study each L separately, which considerably reduces the set of basis vectors needed in each computation.

We choose the one-pair-state basis functions as

$$\tilde{\Phi}_{n_1n_2l_1l_2;LM}^{(1)}(r_e,r_h)=\sum_{m_1m_2}\langle l_1m_1l_2m_2|LM\rangle \times\phi_{N_1}(r_e)\phi_{N_2}(r_h) \ , \quad (16)$$

where $\langle l_1m_1l_2m_2|LM\rangle$ is the Clebsch-Gordan coefficient in Condon-Shortley notation.[18] L and M label the eigenstates of interest.

The four particles representing a two-pair state can be arranged in pairs. There are a number of equivalent ways to generate the basis. One basis can be transformed into another one by a unitary transformation, without influencing the eigenstates and eigenvalues. In order to make use of some symmetry properties in our numerical calculations, we couple electron pair and hole pair separately and then couple all pairs together to get the total angular momentum. We define the basis for our two-electron-hole-pair states as

$$\tilde{\Phi}^{(2)}_{n_1n_2n_3n_4;l_1l_2l_3l_4;LM}(r_{e_1},r_{e_2},r_{h_1},r_{h_2})=\sum_{m_em_hm_1,m_2,m_3,m_4}\langle l_em_el_hm_h|LM\rangle\langle l_1m_1l_2m_2|l_em_e\rangle\langle l_3m_3l_4m_4|l_hm_h\rangle$$

$$\times\phi_{N_1}(r_{e_1})\phi_{N_2}(r_{e_2})\phi_{N_3}(r_{h_1})\phi_{N_4}(r_{h_2})\ . \tag{17}$$

In the following paragraphs we now discuss some relevant details of our numerical techniques. The kinetic-energy parts of the Hamiltonian matrices are trivial so we concentrate on the Coulomb matrix elements. The basis for one- and two-pair states are superpositions of $\{\Phi_1\}$ and $\{\Phi_2\}$ in Eqs. (15) and (16), respectively. In both cases the matrix elements are therefore related to

$$\int\int d^3r_1d^3r_2[\Phi^{(1)}_{N_1,N_2}(r_1,r_2)]^*\frac{e^2}{\epsilon_2|r_1-r_2|}\Phi^{(1)}_{N_1',N_2'}(r_1,r_2)$$

$$=2E_R\left[\frac{a_B}{R}\right]\int_0^1\int_0^1 dx_1dx_2x_1^2x_2^2\int\int d\Omega_1d\Omega_2\frac{R^6\phi^*_{N_1}(Rx_1)\phi_{N_1'}(Rx_1)\phi^*_{N_2}(Rx_2)\phi_{N_2'}(Rx_2)}{|x_1-x_2|}\ , \tag{18}$$

where ϵ_2 is the background dielectric constant inside the quantum dot. Because of the definition of $\phi_N(r)$ by Eq. (8) the integral on the right-hand side is independent of R. In order to evaluate the integrals in Eq. (18), we use the expansion formulas

$$\frac{1}{|r_1-r_2|}=\sum_l\frac{1}{r_>}\left[\frac{r_<}{r_>}\right]^l P_l(\cos\gamma)$$

and

$$P_l(\cos\gamma)=\frac{4\pi}{2l+1}\sum_{m=-l}^{l}Y^*_{lm}(\theta_1\phi_1)Y_{lm}(\theta_2\phi_2)\ , \tag{19}$$

where $r_>(r_<)$ is the larger (smaller) radius among $|r_1|$ and $|r_2|$. Inserting Eq. (19) into Eq. (18), the integral can be decomposed into two parts, one containing the radial integrations and the other one containing the angular integrals. The angular part is

$$\int d\Omega_1Y_{l_1m_1}(\Omega_1)Y^*_{l_1'm_1'}(\Omega_1)Y_{lm}(\Omega_1)$$
$$\times\int d\Omega_2Y_{l_2m_2}(\Omega_2)Y^*_{l_2'm_2'}(\Omega_2)Y^*_{lm}(\Omega_2)\ .$$

According to results in group theory,[19] integration of three spherical harmonic functions provide selection rules. The angular integral vanishes unless

$$|l_1-l_1'|\le l\le l_1+l_1'\ ;$$
$$m_1-m_1'=m\ ;$$
$$l_1+l_1'+l=\text{even number}\ .$$

In practice, we evaluate the integral $\int d\Omega Y_{l_1m_1}Y^*_{l_1'm_1'}Y_{lm}$ for all possible combinations of $(l_1m_1,l_1'm_1',lm)$ for a given set of basis functions, store the results in a data file, and use that data file repeatedly in the calculations. Similarly, the radial integrals are calculated and stored in a data file. Starting from the lowest quantum numbers, we use for our explicit calculations the first 18 single-particle wave functions. We include angular momentum states up to $l=6$.

For the radial integrals we make also use of some symmetry properties to simplify the numerical calculations. For this purpose it is worthwhile to notice that in Eq. (13) the two electrons (holes) are symmetric and the electron pair is symmetric with the hole pair. For example, the Coulomb matrix elements are equal for the wave function combinations with the indices

$$(N_{e_1}N_{e_2})(N_{h_1}N_{h_2})\equiv(N_1N_2)(N_3N_4)=(N_2N_1)(N_3N_4)$$
$$=(N_3N_4)(N_1N_2)=\cdots\ .$$

Making use of this fact, the radial integrals are calculated numerically only for those states $(N_{e_1}N_{e_2})(N_{h_1}N_{h_2})$ where $N_{e_1}\le N_{e_2}$, $N_{h_1}\le N_{h_2}$, and $N_{e_1}\le N_{h_1}$. For given bra and ket states, we reorder the index configurations to eliminate double computations. In this way, we can reduce the number of spatial integrals to about 15 000.

Again, the extensions from the one-EHP states to two-EHP states are straightforward, although the number of basis functions needed is much larger. The Coulomb interactions in Eq. (13) relate only two of the four particles, allowing to use the Coulomb contributions from the one-pair-state calculations. The Coulomb contributions are all proportional to (a_B/R). In general, one can show that the total matrix elements between the chosen basis states therefore have the form

$$H_{ij}=E_i\delta_{ij}\left[\frac{a_B}{R}\right]^2-C_{ij}\left[\frac{a_B}{R}\right]\ ,$$

where E_i and C_{ij} are independent of the quantum-dot radius.

Employing all the described simplifications, we obtain a set of different matrices representing the various interactions in the system. The total Hamiltonian matrix of the system is then diagonalized numerically, using *IMSL* routines, which provide all the eigenvalues and eigenvectors. The accuracy of these routines exceeds all our requirements.

IV. OPTICAL PROPERTIES OF QUANTUM DOTS

In the previous two sections we discussed the energies and wave functions of quantum-confined electrons and

holes. Now we apply those results to study the linear and nonlinear-optical properties of the QD's. We restrict ourselves to χ^1 and χ^3 for which we need the energies of the eigenstates and the dipole elements between the eigenstates. Phenomenologically we also include relaxation between the states.

Assuming that intraband transitions can be neglected, the polarization is described by the operator P^+ defined by Eq. (3). The relevant dipole matrix elements are those between vacuum and one-pair states and between one-pair states and two-pair states, respectively. For the one-pair-state matrix element we obtain

$$\langle \Psi_{e\text{-}h}|P^+|0\rangle = p_{cv}\sum_s \int dr \langle \Psi_{e\text{-}h}|\psi_e^\dagger(r,s)\psi_h^\dagger(r,s)|0\rangle$$
$$= p_{cv}\int dr[\phi^{(1)}(r,r)]^* \sum_s \chi(s,s) . \quad (20)$$

The spin parts of the wave functions can be chosen so that only one eigenstate (with total spin zero) is coupled to the vacuum and the other three combinations (with total spin one) are not. For the spin-zero state we have the coefficients $\chi(s,s)=(1/\sqrt{2})$ and $\chi(s,-s)=0$. We now expand $\phi^{(1)}$ in terms of the single-particle wave functions $\phi_N(r)$ defined by Eq. (8)

$$\phi^{(1)}(r,r')=\sum_{NN'}\zeta(N,N')\phi_N(r)\phi_{N'}(r') . \quad (21)$$

The coefficients ζ are obtained by the matrix diagonalization. The integral in Eq. (20) is easily done and we obtain the matrix element in the form

$$\langle \Psi_{e\text{-}h}|P^+|0\rangle = \sqrt{2}\sum_N (-1)^m \zeta^*(nlm,nl-m)$$
$$= \sqrt{2}\sum_{nl}\sqrt{2l+1}\tilde{\zeta}^*(nnl)\delta_{L,0} . \quad (22)$$

Here, $\tilde{\zeta}(nn'l)$ is the expansion coefficient if we choose the expansion functions already as eigenfunctions of the total angular momentum in the subspace $L=0$.

Next, we want to calculate the dipole moments between the one- and two-pair states in terms of the coefficients obtained by the matrix diagonalization. As consequences of the diagonalization, the coefficients $\phi^{(2)}$ for the two-pair states are either spatially symmetric, $\phi_s^{(2)}$, or antisymmetric, $\phi_a^{(2)}$, both for the electron and hole coordinates. the spin part then must be chosen correspondingly, so that the total coefficient is independently antisymmetric in both variables. This leads to different combinations, the most important of which is the case when the spatial part is symmetric and the spin part is antisymmetric, because these states are low in energy. We write for the biexciton state

$$|\Psi_2\rangle = \int\int\int\int dr_{e_1}dr_{e_2}dr_{h_1}dr_{h_2}\phi_s^{(2)}(r_{e_1},r_{e_2},r_{h_1},r_{h_2})\psi_e^\dagger(r_{e_1},\tfrac{1}{2})\psi_e^\dagger(r_{e_2},-\tfrac{1}{2})\psi_h^\dagger(r_{h_1},\tfrac{1}{2})\psi_h^\dagger(r_{h_2},-\tfrac{1}{2})|0\rangle , \quad (23)$$

where the spatial part has been normalized to one. Then the dipole matrix element is given by

$$\langle \Psi_2|P^+|\Psi_1\rangle = -\sqrt{2}p_{cv}\int\int\int dr\, dr_e dr_h[\phi_s^{(2)}(r_e,r,r_h,r)]^*\phi^{(1)}(r_e,r_h) .$$

If the spatial wave function is antisymmetric in both electron and hole coordinates, we have two different kinds of functions that are dipole coupled to the one-pair state. One has the form of Eq. (23) (s is replaced by a) and the other is of the form

$$|\Psi_2\rangle = \frac{1}{2\sqrt{2}}\int\int\int\int dr_{e_1}dr_{e_2}dr_{h_1}dr_{h_2}\phi_a^{(2)}(r_{e_1},r_{e_2},r_{h_1},r_{h_2})\sum_s \psi_e^\dagger(r_{e_1},s)\psi_e^\dagger(r_{e_2},s)\psi_h^\dagger(r_{h_1},s)\psi_h^\dagger(r_{h_2},s)|0\rangle ,$$

and the corresponding matrix element is

$$\langle \Psi_2|P^+|\Psi_1\rangle = -2p_{cv}\int\int\int dr\, dr_e dr_h[\phi_a^{(2)}(r_e,r,r_h,r)]^*\phi^{(1)}(r_e,r_h) .$$

In the first case the pairs have opposite spins and in the latter case they have same spins. All other dipole matrix elements, involving a totally antisymmetric spatial part for the two-pair state, are zero. Also those states for which the spatial wave function is antisymmetric in one of the coordinates and symmetric in the other are not dipole coupled.

Now we are in a position to evaluate the optical properties of a quantum dot. When the dot radius is comparable to the Bohr radius of the exciton, the energy levels are well separated, and we assume that the one- and two-pair states are responsible for essentially all optical transitions. Since we assume optical pumping of the system near the lowest one-pair resonance, all the other transitions are off resonance and can be neglected. In the following, we used the density-matrix equations in the basis of the states obtained by the numerical diagonalization. The density-matrix approach is well suited for our present purpose since it allows to include also phenomenological relaxation processes, which is not possible in the wave function formalism. The dynamic equation for the density matrix is given by

$$i\hbar\frac{\partial}{\partial t}\rho=[\hat{H}+\hat{H}_{\rm int},\rho]+L_R(\rho) , \quad (24)$$

where L_R models all dissipative processes, $\hat{H}$ and $\hat{H}_{\rm int}$ represent the relevant parts of the Hamiltonians (1) and (3), respectively. They are given in the form

$$\hat{H}=\sum_e \hbar\omega_e P_{ee}+\sum_b \hbar\omega_b P_{bb}$$

and

$$\hat{H}_{\rm int}=-\hbar\sum_e \mu_{e0}E(t)P_{e0}-\hbar\sum_{eb}\mu_{be}E(t)P_{be}+\text{H.c.}\ ,$$

where the indices 0, e, and b refer to the vacuum, one-pair and two-pair states, respectively. The operators P_{ij} are projectors which in the bra-ket formalism have the form $|i\rangle\langle j|$. The dipole matrix elements are $\mu_{e0}=\langle\Psi_1|P^+|0\rangle$ and $\mu_{be}=\langle\Psi_2|P^+|\Psi_1\rangle$.

In the following, we calculate the steady-state optical properties for pump-probe spectroscopy under continuous-wave excitation. An analytic solution of Eq. (24) for more than three levels is very tedious, even for single-beam excitation. Hence, we restrict ourselves to the third-order response χ^3 which can be evaluated analytically. The single-beam excitation was studied in Ref. 9. We write the light field in the form

$$E(t)=E_L e^{-iw_L t}+E_p e^{-iw_p t}\ ,$$

where p stands for probe and L is the pump-laser field. We solve Eq. (24) perturbatively in the field $E(t)$, neglecting all terms containing E_L^3 and E_p^2, or higher powers. The susceptibility is obtained from the total polarization

$$P=\langle P^+\rangle=\sum_e \mu_{e0}\rho_{0e}+\sum_{eb}\mu_{be}\rho_{eb}\ .$$

To analyze the typical pump-probe experiments,[13,15–17] we need that part of the signal which travels in the probe direction. Therefore, we compute only that component P_p from P which is proportional to $E_p^*(t)$. The pump-probe susceptibility $\chi_p(\omega_p)$ is then determined by the equation

$$P_p=\chi_p(\omega_p)E_p^* e^{i\omega_p t}\ .$$

The part of χ_p which is independent of the pump field (zeroth order) yields the linear-absorption and refractive-index spectra. The nonlinear effects are given by the third-order susceptibility $\chi_p^{(3)}$, which is proportional to the intensity of the pump field. Through straightforward, but long algebraic manipulations, we obtain the third-order susceptibility for the probe in the presence of a strong pump as

$$\begin{aligned}\chi_p^{(3)}(\omega_p)\Big|_R = i|E_L|^2\Bigg\{ &\sum_{ee'}\frac{|\mu_{e0}|^2|\mu_{e'0}|^2}{\Gamma_{e0}+i(\omega_e-\omega_p)}\Bigg[\frac{2\Gamma_{e'0}/\Gamma_{e'e'}}{\Gamma_{e'0}^2+(\omega_{e'}-\omega_L)^2}+\left[\frac{1}{\Gamma_{e'0}-i(\omega_{e'}-\omega_L)}+\frac{1}{\Gamma_{e'0}+i(\omega_{e'}-\omega_p)}\right]\\ &\times\frac{1}{\Gamma_{e'e'}-i(\omega_p-\omega_L)}+\frac{1}{\Gamma_{e'0}-i(\omega_{e'}-\omega_L)}\\ &\times\left[\frac{1}{\Gamma_{ee'}+i\omega_{ee'}}+\frac{1}{\Gamma_{ee'}+i(\omega_{ee'}-\omega_p+\omega_L)}\right]\\ &+\frac{1}{\Gamma_{e0}+i(\omega_e-\omega_L)}\frac{1}{\Gamma_{ee'}+i\omega_{ee'}}+\frac{1}{\Gamma_{e0}+i(\omega_e-\omega_p)}\frac{1}{\Gamma_{ee'}+i(\omega_{ee'}-\omega_p+\omega_L)}\Bigg]\\ &+\sum_{bee'}\mu_{0e}\mu_{eb}\mu_{be'}\mu_{e'0}\Bigg\{\frac{1}{\Gamma_{b0}+i(\omega_b-\omega_L-\omega_p)}\left[\frac{1}{\Gamma_{e0}+i(\omega_e-\omega_p)}-\frac{1}{\Gamma_{be}+i(\omega_{be}-\omega_p)}\right]\\ &\times\left[\frac{1}{\Gamma_{e'0}+i(\omega_{e'}-\omega_L)}+\frac{1}{\Gamma_{e'0}+i(\omega_{e'}-\omega_p)}\right]-\frac{1}{\Gamma_{be}+i(\omega_{be}-\omega_p)}\\ &\times\Bigg[\frac{1}{\Gamma_{e0}-i(\omega_e-\omega_L)}\left[\frac{1}{\Gamma_{ee'}-i\omega_{ee'}}+\frac{1}{\Gamma_{ee'}-i(\omega_{ee'}+\omega_p-\omega_L)}\right]\\ &+\frac{1}{\Gamma_{e'0}+i(\omega_{e'}-\omega_L)}\frac{1}{\Gamma_{ee'}-i\omega_{ee'}}\\ &+\frac{1}{\Gamma_{e'0}+i(\omega_{e'}-\omega_p)}\frac{1}{\Gamma_{ee'}-i(\omega_{ee'}+\omega_p-\omega_L)}\Bigg]\Bigg\}\Bigg]\Bigg\}\ .\end{aligned}\tag{25}$$

Here, $\omega_{ij}=\omega_i-\omega_j$, Γ_{ij} for $i\neq j$ is the phenomenological coherence decay rate of the ij transition, and Γ_{ii} describes the population decay of state i, respectively.

V. NUMERICAL RESULTS AND DISCUSSION

In this section we present examples of the numerical evaluation of our results. We concentrate here on the properties of intrinsic semiconductor quantum dots, i.e., we do not consider effects caused by eventual surface charges or by external fields. These modifications are discussed in Ref. 15, where we exactly follow the approach of the present paper, but include additional Coulomb or electric-field terms in the Hamiltonian (1). In all of our results, we give the dot radius in units of the bulk-exciton

Bohr radius and the energies in units of the bulk-exciton Rydberg energy, respectively. Therefore, the presented results are only very weakly material dependent. This dependence enters only through the ratio m_e/m_h of effective electron and hole mass and through the ratio ϵ_2/ϵ_1 of background dielectric constants inside and outside the quantum dot, respectively.

In Fig. 1 we plot the ground-state energy E_1 for one electron-hole pair as function of the quantum-dot radius for $\epsilon_2/\epsilon_1=1$. This figure clearly shows the sharp energy increase for smaller dots expected from the R^{-2} dependence of the confinement energy. To demonstrate the dependence on the electron-hole mass ratio, we show the results for $m_e/m_h=1$ and $m_e/m_h=0.01$, respectively. We obtain relatively minor energy differences, which are most pronounced in the size regime $1<R/a_0<4$, and clearly negligible for $R/a_0<1$.

To demonstrate the influence of the electron-hole Coulomb interaction on the one-pair state, we compare in Fig. 2 the radial distribution

$$Pr_e=r_e^2\int\int\int d\Omega_e d\Omega_h dr_h r_h^2|\phi^{(1)}(r_e,r_h)|^2 \tag{26}$$

of electron and hole ($e\leftrightarrow h$) in the quantum dot with the strong-confinement situation without Coulomb interaction. [$d\Omega$ in Eq. (26) denotes the angular integration.] For the results plotted in Fig. 2 we choose the mass ratio

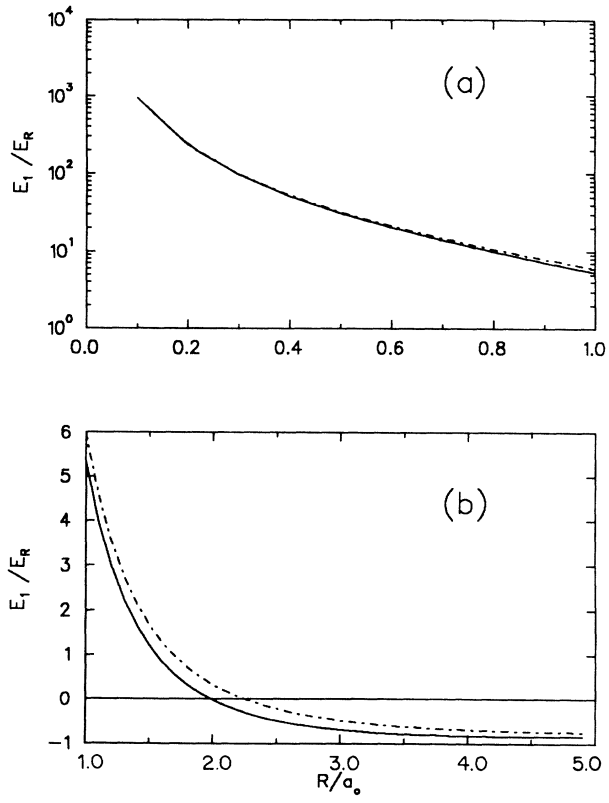

FIG. 1. Ground-state energy E_1 for one electron-hole pair as function of the quantum-dot radius for $\epsilon_2/\epsilon_1=1$, $m_e/m_h=1$ (dashed line), and $m_e/m_h=0.01$ (solid line). (a) shows the range $0\le R/a_0\le 1$ and (b) shows the results for $R/a_0\ge 1$, respectively.

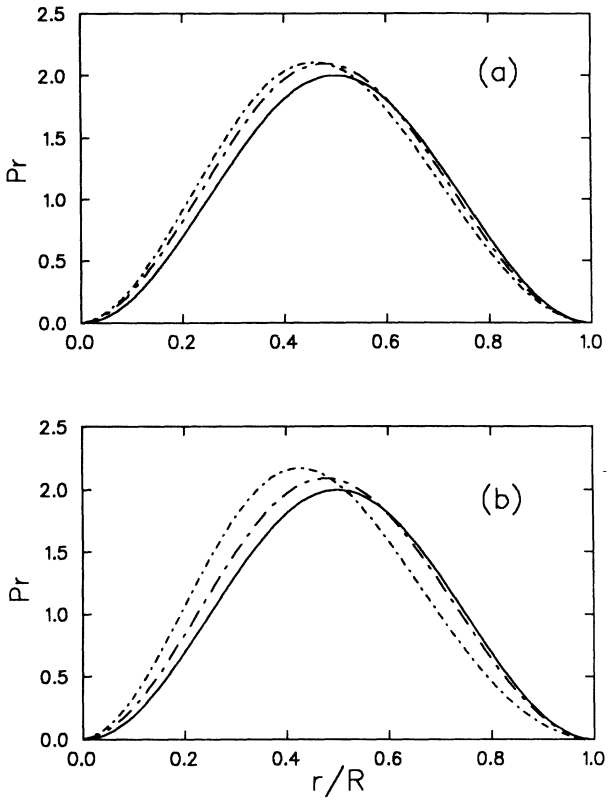

FIG. 2. Radial distribution, Eq. (26), for one electron-hole pair in the quantum dot. The short-dashed line is the hole distribution, the long-dashed line is the electron distribution, and the solid line shows the strong-confinement result without Coulomb interaction, which is identical for electron and hole. (a) and (b) show the results for $R/a_0=0.5$ and $R/a_0=1$, respectively.

$m_e/m_h=0.24$, which is reasonable, e.g., for CdSe quantum dots. We see that, as a consequence of the electron-hole Coulomb interaction, the heavier particle, i.e., the hole, is pushed toward the center of the sphere. This effect is more pronounced for $R/a_0=1$ [Fig. 2(b)] than for $R/a_0=0.5$ [Fig. 2(a)]. However, even for $R/a_0=0.5$, the differences between the "true" radial distribution and the strong-confinement approximation are still quite significant.

In Fig. 3 we show the biexciton binding energy δE_2, Eq. (14), as function of dot radius for three different electron-hole mass ratios and $\epsilon_2/\epsilon_1=1$. The solid lines are the results of our numerical matrix diagonalization, and the dashed curves are computed using third-order perturbation theory. We find, that independent of the electron-hole mass ratio, the biexciton binding energy increases with decreasing dot radius. For the physically unrealistic, but theoretically interesting limit $R\to 0$, we see that the ground-state biexciton energy approaches values of one to two times the exciton binding energy in the bulk. We checked these results also for different ratios of ϵ_2/ϵ_1 and always found qualitatively the same behavior. As discussed in Ref. 16, we therefore conclude, that Coulomb effects are important, even for the smallest quantum dots.

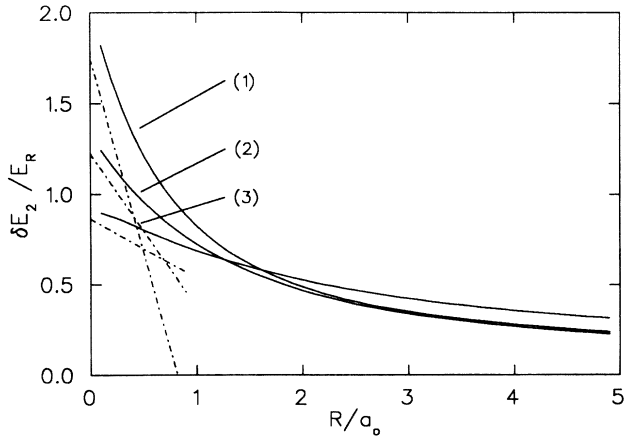

FIG. 3. Biexciton binding energy δE_2 as function of dot radius for three different electron-hole mass ratios and $\epsilon_2/\epsilon_1=1$. The solid lines are the result of the numerical matrix diagonalization for $m_e/m_h=0.1$ (curve 1), 0.2 (curve 2), 1 (curve 3), and the dashed curves are computed using third-order perturbation theory, respectively.

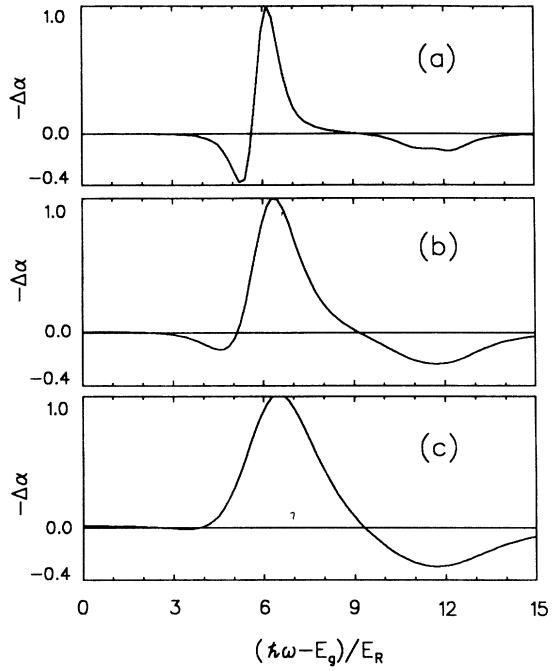

FIG. 4. Change in optical transmission, $-\Delta\alpha$, computed from the imaginary part of χ_3, Eq. (25), as function of probe-energy detuning from the bulk semiconductor band gap E_g (in units of the bulk-exciton Rydberg energy E_R). The shown results are for $R/a_0=1$, $\epsilon_2/\epsilon_1=1$, $m_e/m_h=0.24$, and all damping constants (a) $\hbar\Gamma_{ij}=\gamma=E_R$; (b) $\gamma=2E_R$; and (c) $\gamma=3E_R$, respectively.

Detailed investigations show that the negative value for δE_2 obtained in Ref. 9 is a direct consequence of the effective Coulomb potential approximation in which the two holes are assumed to move in the average potential of the electrons. Our new numerical solution shows that the biexciton binding energy is always negative, giving clear evidence that the effective Coulomb potential used in Ref. 9 is not sophisticated enough to properly include all the important electron-hole correlation effects. Furthermore, we have to realize that the variational evaluations of the biexciton binding energy δE_2 presented in Ref. 11 are very unreliable, especially for small quantum-dot radii. To arrive at this conclusion, we compared the results of our matrix diagonalization with the variational findings of Ref. 8 for the exciton energy E_1. We find excellent agreement showing that the chosen variational wave function is very good to obtain the ground-state properties of a single electron-hole pair in a quantum dot. The same cannot be said, however, concerning the biexcitonic wave function used in Ref. 11. Since the parameter γ has been fixed to be unity (see p. 10 214 of Ref. 11), the variational function [Eq. (2.3) in Ref. 11] cannot approach the strong confinement wave function in the limit for $R\rightarrow 0$. Probably this is the reason for the nonmonotonic behavior and sign change of δE_2 shown, e.g., in Figs. 1 and 2 of Ref. 11, which is in clear contradiction to the analytically shown limit $\delta E_2>0$ for $R\rightarrow 0$.[14] As already pointed out in Ref. 14, variational calculations for the biexciton binding energy may give incorrect results since this method only yields upper bounds for the one- and two-pair energies, without the possibility to control the accuracy of the energy differences.

Figure 4 shows the change in optical transmission, $-\Delta\alpha$, of a quantum-dot sample which is proportional to the imaginary part of the susceptibility, Eq. (25). The parameters are $R/a_0=1$, $\epsilon_2/\epsilon_1=1$, and $m_e/m_h=0.24$. In Figs. 4(a)–4(c) we present the results for the frequency regime around the lowest exciton resonance E_1 for different damping constants $\hbar\Gamma_{ij}=\gamma$. [For simplicity we took all damping constants in Eq. (25) equal, since the properties of the energetically higher transitions do not appreciably influence the results in the frequency regime shown in Fig. 4.] We assumed a pump frequency ω_L given by $(\hbar\omega_L-E_g)=6.2E_R$, which corresponds to the energy E_1 of the energetically lowest one-pair state. Figure 4 shows a positive peak around the pump frequency, indicating the saturation (bleaching) of the one-pair transition. Additionally, we see negative structures on the low- and high-energy side of the positive peak. These negative peaks show increasing probe absorption due to the generation of two-electron–hole-pair states via absorption of one pump and one probe photon. The resonance on the low-energy side of the positive peak is caused by the ground-state biexciton and is known from bulk semiconductors, such as CuCl, which have a large biexciton binding energy. Figure 4 shows that this resonance is visible in quantum dots only for relatively small broadening γ. It is suppressed by the saturating one-pair resonance for increasing γ.

The induced absorption on the high-energy side of the saturating one-pair resonance is caused by transitions to excited-state biexcitons. These transitions are possible since the Coulomb interaction changes the selection rules for dipole transitions. Taking a closer look at the possible excited two-pair states shows that the energetically lowest of these states are actually those where one or two of the heavier holes are not in their ground state. The

relevant examples are where the main quantum numbers of the state (e_1,e_2,h_1,h_2) are $n=(1,1,1,1)$, $l=(0,0,1,1)$, and $n=(1,1,1,2)$ and $l=(0,0,0,0)$, respectively. These pure product states could not make a dipole transition to the one-pair state. In reality, however, such a transition becomes possible since the Coulomb interaction causes a mixing of the independent particle states. In simple terms, one can explain this induced absorption as a consequence of the symmetry breaking through the presence of the pump-generated electron-hole pair. In this situation, the probe photon generates an electron-hole pair in the presence of the pump-generated pair. Since the Coulomb interaction changes the dipole selection rules, the possibilities for dipole transitions involving the probe photon are different than those of the pump photon. In this sense, the induced absorption resembles the "excited-state absorption" in atomic physics. This induced absorption on the high-energy side of the saturating one-pair resonance has been observed in several quantum-dot samples.[13,16,17]

In Fig. 5 we show the computed pump-induced transmission changes for $R/a_0=0.5$, $m_e/m_h=0.24$, $\hbar\gamma=10E_R$ for $\epsilon_2/\epsilon_1=1$ [Fig. 5(a)], and $\epsilon_2/\epsilon_1=10$ [Fig. 5(b)]. The insets show the one- and two-pair dipole transition matrix elements as dashed and full lines, respectively. One clearly sees the ground-state biexciton on the low-energy side of the lowest one-pair state, as well as the higher biexciton states energetically between the two lowest one-pair resonances. As shown in Fig. 4 the assumed relatively large homogeneous broadening in Fig. 5 leads to the suppression of the increasing absorption for the ground-state biexciton. However, the increasing absorption due to the excited-state biexcitons is clearly visible. In fact, this induced absorption feature is even enhanced through the surface polarization effects, which are present in Fig. 5(b). These additional Coulomb terms increase the differences between our results and those of the strong-confinement approximation. Therefore, they help to make the induced absorption feature more pronounced. Similar conclusions have also been reached in Ref. 15, where we additionally included the effects of traps or charged impurity states. The inset of Fig. 5 shows the energetic position and the normalized oscillator strengths of the one- and two-pair transitions.

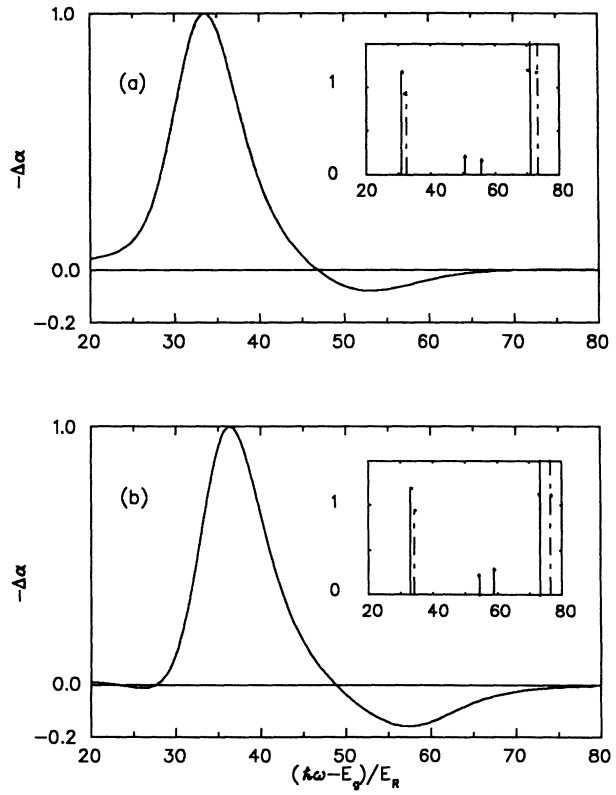

FIG. 5. Same as Fig. 4, but for $R/a_0=0.5$, $\gamma=10E_R$, and (a), $\epsilon_2/\epsilon_1=1$ and (b), $\epsilon_2/\epsilon_1=10$. The insets show the energetic position and the normalized oscillator strengths of the one- and two-pair transitions as dashed and solid lines, respectively.

In summary, we have presented a numerical scheme to compute the one- and two-electron–hole-pair states with the accuracy limited only by available compute time or storage capacity. We show that Coulomb effects are important even in the smallest quantum dots, leading to a biexciton binding energy which increases with decreasing dot size. The Coulomb interaction is responsible also for modifications of the optical dipole transitions, causing a pronounced induced absorption feature on the high-energy side of the saturating one-pair resonance. Our approach can be extended to include the effects of interactions with impurities and/or traps which may be present in realistic samples.[15]

ACKNOWLEDGMENTS

This work has been supported by grants from the National Science Foundation (Washington, D.C.) (NSF), the Optical Circuitry Cooperative at the University of Arizona, and a NATO travel grant.

APPENDIX

For very small radii, $R\rightarrow 0$, the matrix diagonalization method suffers from the fact that the diagonal elements become so dominant that corrections to the strong-confinement results may become inaccurate. In Ref. 14, standard second-order perturbation theory in the Coulomb interaction has been used to show for $R\rightarrow 0$ that the binding energy of the biexciton is finite and positive. To have an independent check for the matrix diagonalization results in the small-radius limit, we extended the treatment of Ref. 14 to third order. The resulting perturbative energies are

$$E_k^{(2)}=\sum_{n\neq k}\frac{|\langle k|\hat{H}_c|n\rangle|^2}{E_k^0-E_n^0}\ , \tag{A1}$$

$$E_k^{(3)}=\sum_{n\neq k}\left[\sum_{m\neq k}\frac{\langle k|\hat{H}_c|m\rangle\langle m|\hat{H}_c|n\rangle\langle n|\hat{H}_c|k\rangle}{(E_k^0-E_m^0)(E_k^0-E_n^0)}-\frac{\langle k|\hat{H}_c|k\rangle|\langle k|\hat{H}_c|n\rangle|^2}{(E_k^0-E_n^0)^2}\right],$$

where $\hat{H}_c$ is the total Coulomb interaction and the indices k, n, and m refer to the eigenstates in absence of the Coulomb interaction, i.e., the strong-confinement eigenfunctions. Because $\langle k|\hat{H}_c|n\rangle$ has the form v/R (v independent of R) and E_k^0 has the form ϵ/R^2 (ϵ independent of R) the perturbation expansion to the eigenenergies is also an expansion in powers of R. We have the general behavior $E_k^{(i)}=\epsilon' R^{i-2}$ (ϵ' independent of R). Inserting Eqs. (5)–(7) into Eq. (10), we find that the biexciton binding energy has the form

$$\delta E_2=\Delta_1-\Delta_2 R+O(R^2)\ ,$$

where Δ_1 and Δ_2 are independent of R. These quantities are given by

$$\Delta_1=2E_{1p}^{(2)}-E_{2p}^{(2)}=\sum_{N,N'\neq 0}|U(N,N')|^2\left[\frac{1}{E_N^e+E_{N'}^e-2E_0^e}+\frac{1}{E_N^h+E_{N'}^h-2E_0^h}+\frac{2}{E_N^e+E_{N'}^h-E_0^e-E_0^h}\right]\ , \tag{A2}$$

where the coefficient $U(N,N')$ is given by

$$\int\int d^3r_1 d^3r_2[\Phi_{0,0}^{(1)}(r_1,r_2)]^*\frac{1}{|r_1-r_2|}\Phi_{N,N'}^{(1)}(r_1,r_2)$$

and

$$\Delta_2 R=E_{2p}^{(3)}-2E_{1p}^{(3)}\ .$$

Equation (A2) shows that the value of Δ_1 is always positive.[14] We find numerically that also $\Delta_2>0$. For the corresponding eigenfunctions we obtain up to second order

$$\psi_k\cong\psi_k^{(0)}+\sum_{n\neq k}\frac{\langle n|\hat{H}_c|k\rangle}{(E_k^{(0)}-E_n^{(1)})}\psi_n^{(0)}+\left[\sum_{\substack{m\neq k\\ n\neq k}}\frac{\langle m|\hat{H}_c|n\rangle\langle n|\hat{H}_c|k\rangle}{(E_k^{(0)}-E_m^{(0)})(E_k^{(0)}-E_n^{(0)})}-\frac{\langle m|\hat{H}_c|k\rangle\langle k|\hat{H}_c|k\rangle}{(E_k^{(0)}-E_m^{(0)})^2}\right]\psi_m^{(0)}-\frac{\psi_k^{(0)}}{2}\sum_{n\neq k}\frac{|\langle n|\hat{H}|k\rangle|^2}{(E_k^{(0)}-E_n^{(0)})^2}\ . \tag{A3}$$

[1] Al. L. Efros and A. L. Efros, Sov. Phys. Semicond. **16**, 772 (1982).

[2] L. E. Brus, J. Chem. Phys. **80**, 4403 (1984); IEEE J. Quantum Electron. **QE-22**, 1909 (1986).

[3] A. I. Ekimov, A. L. Efros, and A. A. Onushchenko, Solid State Commun. **56**, 921 (1985).

[4] N. F. Borrelli, D. W. Hall, H. J. Holland, and D. W. Smith, J. Appl. Phys. **61**, 5399 (1987).

[5] W-Y. Wu, J. N. Schulman, T. Y. Hsu, and U. Efron, Appl. Phys. Lett. **51**, 710 (1987).

[6] E. Hanamura, Solid State Commun. **62**, 465 (1987); Phys. Rev. B **37**, 1273 (1988).

[7] S. Schmitt-Rink, D. A. B. Miller, and D. S. Chemla, Phys. Rev. B **35**, 8113 (1987); Adv. Phys. **38**, 89 (1989).

[8] Y. Kayanuma, Phys. Rev. B **38**, 9797 (1988).

[9] L. Banyai, Y. Z. Hu, M. Lindberg, and S. W. Koch, Phys. Rev. B **38**, 8142 (1988).

[10] P. Roussignol, D. Ricard, C. Flytzanis, and N. Neuroth, Phys. Rev. Lett. **62**, 312 (1989).

[11] T. Takagahara, Phys. Rev. B **39**, 10 206 (1989).

[12] Y. Wang, N. Herron, W. Mahler, and A. Sune, J. Opt. Soc. Am. **6**, 808 (1989).

[13] N. Peyghambarian, S. H. Park, R. A. Morgan, B. Fluegel, Y. Z. Hu, M. Lindberg, S. W. Koch, D. Hulin, A. Migus, J. Etchepare, G. Grillon, D. W. Hall, and N. F. Borrelli, in *Optical Switching in Low-Dimensional Systems,* edited by H. Haug and L. Banyai (Academic, New York, 1989).

[14] L. Banyai, Phys. Rev. B **39**, 8022 (1989).

[15] S. H. Park, R. A. Morgan, Y. Z. Hu, M. Lindberg, S. W. Koch, and N. Peyghambarian, J. Opt. Soc. Am. B (to be published).

[16] Y. Z. Hu, S. W. Koch, M. Lindberg, N. Peyghambarian, R. Pollock, and F. F. Abraham, Phys. Rev. Lett. **64**, 1805 (1990).

[17] N. Peyghambarian, B. Fluegel, D. Hulin, A. Migus, M. Joffre, A. Antonetti, S. W. Koch, and M. Lindberg, IEEE. J. Quantum Electron. **QE-25**, 2516 (1989).

[18] E. U. Condon and G. H. Shortley, *The Theory of Atomic Spectra* (Cambridge University Press, London, 1951).

[19] See, e.g., E. P. Wigner, *Group Theory and its Applications to Quantum Mechanics* (Academic , New York, 1959).